

GIS-assisted modelling for debris flow hazard assessment based on the events of May 1998 in the area of Sarno, Southern Italy. Part II: Velocity and Dynamic Pressure

Journal:	<i>Earth Surface Processes and Landforms</i>
Manuscript ID:	ESP-05-0073.R1
Wiley - Manuscript type:	Paper
Date Submitted by the Author:	12-Oct-2007
Complete List of Authors:	Toyos, Guillermo; University of Cambridge, Geography Gunasekera, Rashmin; Coventry University, Geography Zanchetta, Giovanni; Universita di Pisa, Scienze della Terra Oppenheimer, Clive; University of Cambridge, Geography Sulpizio, Roberto; Universita di Bari, Geomineralogico Favalli, Massimiliano; Istituto Nazionale di Geofisica e Vulcanologia (INGV), SIG Pareschi, Maria Teresa; Istituto Nazionale di Geofisica e Vulcanologia (INGV), SIG
Keywords:	debris flows, GIS, hazard assessment, mobility, velocity



1
2 **Full title:** GIS-assisted modelling for debris flow hazard assessment based on the events of May 1998
3
4 in the area of Sarno, Southern Italy. Part II: Velocity and Dynamic Pressure.

5
6 **Short title:** GIS-assisted modelling of debris flow velocity and dynamic pressure

7
8 **Authors:** Toyos G¹, Gunasekera R², Zanchetta G³; Oppenheimer C¹; Sulpizio R⁴, Favalli, M⁵, Pare-
9
10 schi MT⁵

11
12 **Affiliations:**

- 13
14
15 1. Department of Geography, University of Cambridge, Cambridge, England
16
17 2. Willis Research Network (WRN), Willis Ltd, London, England
18
19 3. Dipartimento di Scienze della Terra, via Santa Maria 53, 56126, Pisa, Italy
20
21 4. CIRISIVU, c/o Dipartimento Geomineralogico, via Orabona 4, 70125, Bari, Italy
22
23 5. Istituto Nazionale di Geofisica e Vulcanologia (INGV), via della Faggiola 31, 56126, Pisa, Italy
24
25

26 **Correspondence author:** Dr. Guillermo Toyos

27
28 **Correspondence address:**

29
30 Comisión Nacional de Actividades Espaciales (CONAE)

31
32 Av. Paseo Colón 751

33
34 1063 – Buenos Aires

35
36 Argentina

37
38 Tel: +54 11 4331 0074 ext. 246

39
40 E-mail: gtoyos@conae.gov.ar, wtoyos@hotmail.com
41
42
43
44
45
46
47
48
49
50
51
52
53
54
55
56
57
58
59
60

Abstract

The velocity and dynamic pressure of debris flows are critical determinants of the impact of these natural phenomena on infrastructure. Therefore, the prediction of these parameters is critical for hazard assessment and vulnerability analysis. We present here an approach to predict the velocity of debris flows on the basis of the energy line concept. First, we obtained empirically- and field-based estimates of debris flow peak discharge, mean velocity at peak discharge and velocity at channel bends and within the fans of ten of the debris flow events that occurred in May 1998 in the area of Sarno, Southern Italy. We used this data to calibrate regression models that enable the prediction of velocity as a function of the vertical distance between the energy line and the surface. Despite the complexity in morphology and behaviour of these flows, the statistical fits were good and the debris flow velocities can be predicted with an associated uncertainty of $< 30\%$ and $< 3 \text{ m s}^{-1}$. We wrote code in Visual Basic for Applications (VBA) that runs within ArcGIS® to implement the results of these calibrations and enable the automatic production of velocity and dynamic pressure maps. The collected data and resulting empirical models constitute a realistic basis for more complex numerical modelling. In addition, the GIS-implementation constitutes a useful decision-support tool for real-time hazard mitigation

Keywords: debris flows, mobility, velocity, GIS, hazard assessment

INTRODUCTION

Debris flows are one of the principal causes of loss of life and property around the world such as in the Vargas Region, Venezuela, in December 1999, where 30,000 people were killed (e.g. García *et al.*, 2003) or in town of Armero, Colombia, where debris flows from Volcán Nevado del Ruiz in 1985 resulted in the complete devastation of the town and 25,000 fatalities (e.g. Pierson *et al.*, 1990). In May 1998 in the Sarno area, Southern Italy, heavy rainfall triggered the failure of volcanic deposits and generated debris flows that affected 5 villages (Figure 1) and killed more than 150 people (Calcaterra *et al.*, 2000; Porfido *et al.*, 2002; Pareschi *et al.*, 2000; Toyos *et al.*, 2003). These events were of relatively low magnitude (de Riso *et al.* 1999; Zanchetta *et al.*, 2004; Toyos *et al.*, 2007_b) but their tragic consequences emphasise the need for improved methods for risk assessment and management. As with the case of pyroclastic density currents (Valentine, 1998; Baxter, 2000; Zuccaro *et al.*, 2000; Spence *et al.*, 2004; Toyos *et al.*, 2007_a) the velocity and dynamic pressure of debris flows are important constraints on their impact on infrastructure (Zhang, 1993; Mizuyama and Ishikawa, 1990; Zanchetta *et al.*, 2004). Therefore, the quantification of these physical parameters is crucial for debris flow hazard assessment and vulnerability analysis.

The efforts to explain and predict debris flow behaviour have traditionally involved the development of rheological models, where the mass and momentum balance equations are solved using some type of relationship between shear stress and strain rate (e.g. Johnson, 1984; Macedonio and Pareschi, 1992; O'Brien *et al.*, 1993; Ayotte and Hungr, 2000). The macroscopic behaviour of debris flows may be also reproduced with a two-parameter Voelmy type model, where the resisting stress at the base is parameterised by a sliding friction and a rate-dependant turbulent term (Körner, 1976; Ayotte and Hungr, 2000; Hungr *et al.*, 2005; Rickenmann, 2005) or with one-dimensional flow-routing models, where the energy dissipation is parameterised by a single roughness coefficient, e.g. Manning *n* (Chow, 1959; Pierson, 1995; Rickenmann and Koch, 1997). Lately, Iverson (2003) developed an alternative to fixed-rheology models that is able to describe the behaviour of the mixture from the onset of motion through deposition and post-depositional consolidation, with no definition of rheological pa-

1
2 parameters required (see also Iverson 1997; Iverson and Denlinger, 2001; Denlinger and Iverson, 2001;
3
4 and Rickenmann, 2005 for a useful review).
5
6
7

8
9 Empirically-based methodologies may be also used to predict the parameters necessary to quantify the
10 destructive power of debris flows. The mobility ratio ($\Delta H/L$) can be used for run-out distance predic-
11 tion (Corominas, 1996; Iverson, 1997; Rickenmann, 1999; Toyos et al., 2007b) and first order ap-
12 proximations of velocity histories of debris flows (e.g. Malin and Sheridan, 1982). The principle is
13 that the ratio between the vertical descent of the gravity-driven mass (ΔH) and the run-out distance (L)
14 can be used to parameterise a friction parameter commonly known as the Heim coefficient (Hsü, 1975;
15 Malin and Sheridan, 1982). This is the energy line concept, originally conceived for rock avalanches
16 by Heim (1882), redefined by Hsü (1975) and further extended to other gravity driven phenomena
17 such as debris flows (Iverson, 1997), pyroclastic flows (Malin and Sheridan, 1982; Sheridan and Ma-
18 lin, 1983; Hayashi and Self, 1992) and debris avalanches (Siebert, 1984). This concept has been ex-
19 panded to incorporate the effects of viscosity and turbulence in the parameterisation of flow shear re-
20 sistance (McEwen and Malin, 1989; Sheridan and Macías, 1992; Kover, 1995) and further
21 implemented for the production of digital maps of maximum flow potential run-out and velocity (e.g.
22 Sheridan *et al.*, 2000; Toyos *et al.*, 2007a). Finally, Rickenmann (1999) provides an overview of em-
23 pirical relationships that can be used to estimate the main parameters of debris flow behaviour, which
24 include maximum discharge rate, mean flow velocity, travel distance and the run-out distance on the
25 fan.
26
27
28
29
30
31
32
33
34
35
36
37
38
39
40
41
42
43
44
45
46
47
48
49
50
51
52
53
54
55
56
57
58
59
60

Although empirical-statistical approaches may not be as accurate as physical models in representing
the true complexity of debris flows and must be applied to conditions similar to those for which they
were developed (Rickenmann, 2005), this kind of methodologies can be particularly useful in situa-
tions such as in the onset of a crisis, when decision making needs to be fast (Malin and Sheridan,
1982). To this end, this paper develops an approach to predict the velocity of debris flows and to pro-
duce digital cartography of debris flow velocity and dynamic pressure. On the basis of the energy line
concept (Hsü, 1975; Malin and Sheridan, 1982) we calibrated equations with empirically- and field-
based estimates of peak discharge, mean velocity at peak discharge, and debris flow velocity within

1
2 the fans (Rickenmann, 1999) of many of the events at Sarno (Figure 1). We implemented these equa-
3 tions with code written in Visual Basic for Applications (VBA) that runs within ArcGIS ® to enable
4 the automatic production of first order velocity and dynamic pressure maps. This code is nested to-
5 gether with another piece of software that enables the prediction of the mobility ratio ($\Delta H/L$) or Heim
6 coefficient (Hsü, 1975; Malin and Sheridan, 1982; Iverson, 1997) and the mapping of the run-out of
7 debris flows, which has been published in a companion paper (Toyos *et al.*, 2007b). While the col-
8 lected data and resulting methodology provide a useful basis for more complex numerical modelling,
9 the GIS-implementation constitutes a useful tool for decision-support and real time hazard mitigation.
10
11
12
13
14
15
16
17
18
19
20
21

22 THE STUDY AREA

23
24
25
26 The study area is a marginal portion of the Apennine belt bordered on the SW side by the Campanian
27 Plain graben and centred on the highlands of Sarno, 20 km east of the Somma-Vesuvius volcano (Fig-
28 ure 1). This is the Pizzo d'Alvano massif composed of Meso-Cenozoic carbonate rocks (Pescatore and
29 Ortolani, 1973) and mantled with loose to poorly consolidated volcanoclastic deposits deriving mainly
30 from the explosive activity of Mt. Somma-Vesuvius (Calcaterra *et al.*, 2000; Pareschi *et al.*, 2002;
31 Crosta and Dal Negro, 2003). The transition between the hill-slopes and the alluvial plains is com-
32 posed by two sets of alluvial fans. The oldest one developed during the late Pleistocene and the
33 youngest one, which is still active, during the Holocene (Di Vito *et al.*, 1998; Pareschi *et al.*, 2000).
34 Stratigraphic data show how volcanoclastic debris flows deposits predominate in both sets of alluvial
35 fans (Zanchetta *et al.*, 2004).
36
37
38
39
40
41
42
43
44
45
46
47
48
49

50 After intense rains (Onorati *et al.* 1999) and a very wet season, on 5 and 6 May 1998, hundreds of
51 landslides coalesced and mobilised as debris flows affecting the areas of Episcopio and Lavarate and
52 the towns of Quindici, Siano and Bracigliano (Figure 1) (Pareschi *et al.*, 2000; Zanchetta *et al.*, 2004),
53 and the Clanio valley (Pareschi *et al.*, 2002). Debris flows reached the piedmont areas and caused the
54 death of more than 150 people and extensive damage to property (Calcaterra *et al.*, 2000; Pareschi *et*
55 *al.*, 2000; Porfido *et al.*, 2002; Toyos *et al.*, 2003). Landslides started at the heads of gullies (between
56 700 m and 950 m.a.s.l.) at slope angles of $> 33^\circ - 35^\circ$. Failures occurred and soil slips rapidly trans-
57
58
59
60

1
2 formed in to debris flows (Zanchetta *et al.*, 2004) that moved downstream at speeds of several km h⁻¹
3
4 (Guadagno *et al.*, 1999). The flows progressively increased in volume while moving down-slope. This
5
6 bulking resulted from the addition of water along the channels and the incorporation of material from
7
8 erosion at the channels' perimeter and bases, and from soil collapses along the flanks. Development of
9
10 channelled paths and bulking generally occurred over slopes of 12° - 30°, whereas deposition com-
11
12 monly took place on slopes of < 12°. Fieldwork indicated that below slopes of less than 12° sediment
13
14 entrainment was usually low (Zanchetta *et al.*, 2004).
15
16
17
18
19

20 **EMPIRICAL DATA**

21
22
23
24 The first part of this study comprised the collection of empirical data and the characterisation of the
25
26 velocity profiles of 10 of the events occurred in the study area (Figure 1). We present here estimates of
27
28 peak discharge, mean velocity at peak discharge and velocity at channel bends and within the fans
29
30 based on field data and empirical relationships available from the literature (Pierson, 1995; Ricken-
31
32 mann, 1999).
33
34
35
36

37 ***Maximum discharge rate***

38
39
40
41 We obtained the maximum discharge rate (Q_p) from (Rickenmann, 1999):
42
43
44

$$45 \quad Q_p = 0.1 M^{0.833} \quad (1)$$

46
47
48
49
50 This formula is for granular flows and based on global data, where M is the maximum volume of the
51
52 debris flow. It is also based on debris flow data, where travel distances between the source areas and
53
54 the point of estimation of Q_p was relatively short. The application of this equation to our study is
55
56 valid, since analyses of their sedimentology showed that they were non-cohesive granular flows
57
58 (Zanchetta *et al.*, 2004). Besides, run-out distances were relatively short, at most 2.1 km. It is impor-
59
60 tant to emphasize that we considered the volume of the debris flow as an indicator of the magnitude of
the event, and therefore we use the terms volume and magnitude interchangeably.

1
2
3
4
5
6
7
8
9
10
11
12
13
14
15
16
17
18
19
20
21
22
23
24
25
26
27
28
29
30
31
32
33
34
35
36
37
38
39
40
41
42
43
44
45
46
47
48
49
50
51
52
53
54
55
56
57
58
59
60

As volume estimates (Table 1) we used the flow volumes calculated for the development of the run-out prediction method presented by the companion paper (Toyos *et al.*, 2007_b), where methods and assumptions are explained in detail. Volumes are based on the source areas mapped from aerial photography and an average thickness of the scarp of 1.2 m (Table 1). While the thickness of the volcaniclastic cover spans from 0 to 3 m on the hillsides, it can be greater than 5 m in flatter areas and less than 1 m on the steepest portions (e.g. Calcaterra *et al.*, 2000), the thickness of the scarps of the events of 1998 ranged between 0.5 and 2.0 m (Pareschi *et al.*, 2000; Zanchetta *et al.*, 2004). This has already been observed in the area of Episcopio and reported previously (Zanchetta *et al.*, 2004) and confirmed by the authors of the present paper using control points in the field. The volumes represent the maximum amount of material that collapsed within the source areas and evolved into debris flows and while this may lead to overestimation, it is a valid assumption as we have considered the events as worst-case scenarios. The flows were variable in morphology and therefore, Toyos *et al.* (2007_b) distinguishes between flows of *simple* and *complex* morphology. The former includes flows that were recognisable as single events with a clear source, transport and/or deposition area (e.g. Ep-2) and the latter comprises flows that exhibited indistinguishable transport and/or deposition areas resulting from more than one source, which were assumed to correspond to a single event (e.g. Ep-6) (Table 1) (Figure 1). In the latter case, volumes of the contributing source areas were added and overestimation is justified again, by considering them as worst case scenarios. We assumed the impact of bulking along transport zones on the alluvial fan surface to be negligible (Zanchetta *et al.*, 2004). The short run-out distances of less than 2.0 km constitute a justification for this assumption (Toyos *et al.*, 2007_b).

The results show peak discharges that range between 0.6 and $3.1 \times 10^3 \text{ m}^3 \text{ s}^{-1}$ (Table 1), consistent with observations from other studies conducted elsewhere (e.g. Pierson, 1995; Rickenmann, 1999).

Mean velocity at peak discharge

The mean velocity at peak discharge (v_{max}) was estimated with the relationship proposed by Rickenmann (1999):

$$v_{max} = 2.1 Q_p^{0.33} S^{0.33} \quad (2)$$

where Q_p is the peak discharge and S is the local slope. These estimates were obtained at the end of the source areas, which is defined by the first large break in slope, i.e. the apex of the alluvial fan (Zanchetta *et al.*, 2004; Toyos *et al.*, 2007b), where field evidence indicates that the bulking process ceased.

Although equation 2 is based on an analysis of clear water flows in torrents and gravel-bed rivers, Rickenmann (1999) observed a reasonable agreement between calculated and observed debris flow velocities, with a similar scatter as for clear water flows ($r^2 = 0.70$). Despite the first order nature of this approximation, this is the only way to assess debris flow maximum velocity after the event and in the absence of direct measurements. Velocities at the end of the source areas of Ep-2, Ep-3, Ep-4, Ep-5, Ep-6, Ep-7, Lav-1, Lav-2, Quin-6 and Sia-2 (Figure 1) ranged between 13 and 18 m s⁻¹ (Table 1). These values are also consistent with other measurements (e.g. Pierson, 1995; Rickenmann, 1999) and with the values measured downstream at channel bends and within the fans (Figures 2, 3.a-c, 4.a-b).

Longitudinal velocity profiles

We obtained indirect estimates of debris flow velocity at channel bends:

$$v = [g r_c (h_2 - h_1) / w]^{1/2} \quad (3)$$

and within the fans:

$$v = (2g h)^{1/2} \quad (4)$$

In Equation 3, g is the gravitational acceleration, r_c is the radius of curvature of the bend, $(h_2 - h_1)$ is the difference between the flow height on the outer and inner side flanks of the bend and w is the channel width (Chow, 1959). Equation 4 assumes a complete conversion of the kinetic energy of the

1
2 flow impacting an obstacle (e.g. building) into potential energy (e.g. Pierson, 1995), where h is the dis-
3 tance between the top of the splash mark on the building and the moving mass. According to Iverson
4 *et al.* (1994), the uncertainty of the velocity estimates obtained with Equation 3 is $< 30\%$, while errors
5 of predictions based on equation 4 are $\sim 30\%$. However, Bulmer *et al.* (2002), suggests using a correc-
6 tion coefficient k , where most reasonable value lies between 0.1 and 0.5, with $k = 0.5$ for wetter flows
7 and $k = 0.1$ for slopes $> 14^\circ$. Hungr *et al.* (1984) suggests a value of $k = 0.2$ for design purposes and
8 0.4 to calculate velocity from superelevation data. In the absence of direct measurements and being
9 aware of the error around our velocity estimates, we adopted a conservative value of $k = 1$.

10
11 We normalised the velocities and the distance from the source areas by the maximum recorded at the
12 apex of the alluvial fans, i.e. mean velocity at peak discharge (Table 1), and by the total flow run-out
13 distance (R), respectively. The latter is the fraction of maximum extent, which is defined as the dis-
14 tance between the location of each velocity measurement and the lowermost part of the source area
15 over the total flow run-out. This ratio facilitated the comparison of velocity profiles.

16
17 All the velocity profiles show an exponential deceleration with distance from the source area (Figure
18 2) (e.g. Pierson, 1995; Zanchetta *et al.*, 2004). Three sets of profiles were distinguished: (i) Ep-2, Ep-4
19 and Ep-7, (ii) Ep-5, Ep-6, Ep-3, Lav-1, Quin-6 and Sia-2 and (iii) Lav-2 (Figure 2). In the first group,
20 the velocities made for locations beyond $0.75 R$ are still $> 6 \text{ m s}^{-1}$. The second set represents the *aver-*
21 *age flow behaviour* with velocities decreasing from the maximum down to $< 6 \text{ m s}^{-1}$ also beyond 0.75
22 R . Ep-5 and Ep-6, constitute the best examples of this average behaviour. Finally, Lav-2 shows veloci-
23 ties $< 6 \text{ m s}^{-1}$ prior to $0.75 R$ (Figure 2).

24
25 From the flows of the first group (i) the morphologies of Ep-2 and Ep-4 were simple (see *Maximum*
26 *discharge rate*, Table 1, Figure 1; see also Table 1 in Toyos *et al.* (2007b)) and within the fans the
27 density of infrastructure was low (Figure 3.a). However, the morphology of Ep-7 was complex (Table
28 1, Figure 1). This flow followed a fairly long channel (Figure 1) and as soon as it entered the built-up
29 area, it followed an artificial channel (Figure 3.b) before spreading and inflicting substantial damage to
30 property. Of the velocities recorded in Sia-2, one was unusually high (i.e. 10.5 m s^{-1}). This value was

1
2 measured at the centre of the flow, at the entrance of the built-up area and at a reinforced concrete
3 structure surrounded by a few buildings. A few hundred metres downstream, the density of buildings
4 was high and the velocities were $< 6 \text{ m s}^{-1}$ (Figure 4.b). The morphology of the ‘average’ flows is vari-
5 able (Table 1) and except for Lav-1 and Quin-6, the density of buildings within their paths was sub-
6 stantial (Figures 3, 4). Finally, the morphology of Lav-2 is highly complex (Figure 3.c). This compli-
7 cated the flow zonation in general and especially the identification of the end of the source areas
8 (Toyos *et al.*, 2007b), which may have resulted in uncontrolled errors in the parameterisation of the
9 velocity profiles. For this reason, the data from Lav-2 was excluded from further analysis.

10
11 The density of infrastructure seems to be the main factor responsible for the shape of the velocity pro-
12 files (Figure 2). However, this alone does not explain much of the variability observed in the flow be-
13 haviour. While the low density of infrastructure may explain the gentler profiles of Ep-2 and Ep-4
14 (Figures 2, 3.a), the profile in Ep-7 could reflect the brief constriction of the flow along the artificial
15 channel (Figures 2, 3.b). In this case, the velocity measurements were taken near the artificial channel,
16 where the flow probably had not lost momentum due to the impact with buildings. Finally, while the
17 density of buildings in Lav-1 and Quin-6 (Figures 3.c, 4.a) was low, the velocity data scatter along the
18 average profile (Figure 2).

41 VELOCITY ESTIMATED FROM THE ENERGY LINE CONCEPT

42
43 Following the collection of empirical data and analysis of velocity profiles along the paths, we used
44 the energy line concept (Hsü, 1975; Malin and Sheridan, 1982) to derive a formula for velocity predic-
45 tion. For a particular flow, the mobility ratio or Heim coefficient is the tangent of the angle that forms
46 the energy line with the horizontal (i.e. depression angle) (Figure 5) and the intersection of this line
47 with topography defines the distal limit of the flow. This line should connect the centres of mass of the
48 source area and the flow deposits but for practical reasons the energy line usually links the highest
49 point of the source area with the flow’s distal limit (Iverson, 1997).

1
2 According to Malin and Sheridan (1982), the distance between the energy line and the ground surface
3
4 (Δh) yields an estimate of flow velocity (v) (Figure 5):
5
6

$$7 \quad v = (2g \Delta h)^{1/2} \quad (5)$$

8
9
10
11
12 However, instead of further parameterising the flow's shear resistance to represent viscosity, turbu-
13 lence, etc. (e.g. McEwen and Malin, 1989; Sheridan and Macías, 1992; Kover, 1995; Rickenmann,
14 1995; Ayotte and Hungr, 2000; Sheridan *et al.*, 2000; Hungr *et al.*, 2005), we used our empirical data
15 to calibrate the general form of equation 5:
16
17
18
19
20

$$21 \quad v = a \Delta h^b \quad (6)$$

22
23 where Δh is constrained by the Heim coefficient and $a = (2g)^{1/2}$ and $b = 1/2$ if only the basal friction is
24 considered. The linear form of Equation 6 provides the opportunity to obtain a and b via linear regres-
25 sion analysis:
26
27
28
29
30
31
32
33

$$34 \quad \log(v) = \log(a) + b \log(\Delta h) \quad (7)$$

35
36
37
38
39
40
41 Equation 7 assumes that all the factors that force the flow to stop (i.e. basal friction, viscosity, turbu-
42 lence, surface roughness, etc.) can be accounted for by the coefficients a and b .
43
44
45
46
47
48
49

50 51 52 53 54 55 56 57 58 59 60

STATISTICAL ANALYSIS

The companion paper (Toyos *et al.*, 2007_b) distinguishes between (i) a mobility defined by an energy line that connects the apex of the alluvial fan with the distal limit of the flow and (ii) a mobility defined by an energy line starting at the top of the highest landslide scar. It was shown that the flow volume correlates well only with the mobility of the first group and this relationship was therefore implemented for automatic prediction and mapping of debris flow run-out. The apex of the alluvial fan appeared to be a better proxy of the centre of mass of the source volume of the flow than the highest

1
2 landslide scar, since at the apex the flow is mature and complete, i.e. the maximum volume is reached.
3
4 The reason for the low correlation observed between the volume and mobility of the second group has
5
6 been attributed to the size and range (i.e. only 2 orders of magnitude) of the datasets, since other au-
7
8 thors (Corominas, 1996) found a good correlation but with much larger datasets that spanned many
9
10 orders of magnitude. However, in the present study, to evaluate whether calibration is possible and
11
12 consequently to calibrate a relationship between V and Δh we used both sets of mobility ratios or de-
13
14 pression angles (Table 2). These were used to constrain the vertical distance between the energy line
15
16 and the surface (Δh) at each velocity measurement site (Table 2) and plot the observed velocities (i.e.
17
18 empirical measures of velocities obtained with Equations 3 and 4) against Δh on a logarithmic scale
19
20 (Figure 6.a-b).
21
22
23
24
25

26 *Data scatter*

27
28
29
30 The maximum values of Δh constrained by the second group of mobility ratios (ii) fall at a location
31
32 that coincides roughly with the location of the apex of the alluvial fan. Therefore, the mean velocity at
33
34 peak discharge measured at the apex (Table 1) can be complemented with these maximum values of
35
36 Δh . For the Heim coefficients of the first group (i), however, we had to recalculate the mean velocity
37
38 at peak discharge (Table 2), since at the apex of the alluvial fan the value of Δh is zero. This value in-
39
40 creases downstream from the apex, reaches a maximum at $\sim 0.5R$ and then drops down to zero at R .
41
42 Therefore, we recalculated the mean velocity at peak discharge (Equation 2) a few hundred meters
43
44 downstream from the end of the source area, where the value of Δh is the highest. Thus, these maxi-
45
46 mum velocities are slightly lower than those at the apex (Tables 1, 2) but the values obtained are gen-
47
48 erally consistent with the velocities measured further downstream. This is logical since the slope at
49
50 that location is lower than at the apex. The peak discharge has been assumed to be the same as the one
51
52 estimated at the end of the source area (Table 1).
53
54
55
56
57

58
59 In both datasets two groups of flow events can be discriminated towards lower values of Δh (Figure
60
6.a-b). The former includes Ep-2, Ep-4 and Ep-7, while the latter is composed by the remaining basins
(except for Lav-2, which was not considered). Thus, both plots of v against Δh exhibit a similar pattern

as the one shown by the velocity profiles (Figure 2). We termed the set of flows with lower velocities (i.e. average behaviour) *Group I* and the other one *Group II* (Figure 6.a-b).

Regression results

We obtained four regression models, one for *Group I* and another for *Group II* for each of the datasets based on the two types of mobility considered, i.e. energy line starting at (i) the apex of the alluvial fan and (ii) the highest landslide scar. We termed these models ApexG1, ScarpG1, Apex G2 and ScarpG2.

All regression models were significant ($p < 0.01$). ApexG1 explained almost 50% of the variance; the r^2 of ScarpG1 and ApexG2 was ≥ 0.6 and of Scarp G2 it was 0.9 (Table 3). The intercepts of ApexG1 and ApexG2 differed significantly at a 95% level of confidence and slopes were significantly different but at a 90% level of confidence. On the other hand, the slopes of ScarpG1 and ScarpG2 were statistically indistinguishable and the intercepts of these models differed significantly at the 90% level of confidence. To quantify the average residual of these calibrations we used the average misfit (%):

$$\text{Average misfit (\%)} = \left\{ \sum [(v_a - v_p) \times 100 / v_a]_i \right\} / n \quad (8)$$

and the root mean square error (RMSE):

$$\text{RMSE} = \left\{ \sum [(v_a - v_p)^2 / n] \right\}^{1/2} \quad (9)$$

where v_a is the empirical velocity, v_p is the predicted velocity and n is the number of observations. For the datasets based on energy lines starting at the apex of the alluvial fan, we observed an average residual of 24%, 29% for ApexG1 and 11% for ApexG2. The average root mean square error was 2.3 m s^{-1} , 2.6 m s^{-1} for ApexG1 and 1.1 m s^{-1} for ApexG2. The uncertainties associated to the other two regression models were somewhat lower. The average misfit of ScarpG1 and ScarpG2 together was of 20% and the RMSE of 2.4 m s^{-1} . While the misfit and RMSE of ScarpG1 were of 24% and 2.8 m s^{-1} , respectively, for ScarpG2 these were of 8% and 0.9 m s^{-1} , respectively.

1
2 Thus, we were able to characterise the velocity of the events at Sarno with a set of equations, one cor-
3 responding to flows with distal velocities that were higher and the other to flows with distal velocities
4 lower than 6 m s^{-1} (Figures 2, 3, 4). With regards to the two types of mobility considered regression
5 models improved (i.e. better fits and lower uncertainties) when based on energy lines that started at the
6 top of the scarps (Table 3).
7
8
9
10
11
12

13 14 15 16 17 18 19 20 21 22 23 24 25 26 27 28 29 30 31 32 33 34 35 36 37 38 39 40 41 42 43 44 45 46 47 48 49 50 51 52 53 54 55 56 57 58 59 60

DYNAMIC PRESSURE

The destructive power of debris flows results from the action of hydrodynamic forces, hydrostatic forces and the collision of individual objects carried by the flow (e.g. large boulders, cars, etc.). We decided to focus on the dynamic forces in order to extend the ability of the code by providing the user the ability to generate dynamic pressure maps.

At the impact against a rigid structure, the flow may either form a vertical jet-like bulge or a wave that propagates upstream (Armanini and Scotton, 1993). Under either of these two hypotheses the dynamic overpressure is proportional to the square of the frontal velocity as follows (Keaton, 1990; Armanini and Scotton, 1993; Zhang, 1993; Coussot, 1997):

$$P_{dy} = k \rho_{df} v^2 \quad (10)$$

where P_{dy} is dynamic pressure, k is a constant, which depends on the density of the granular material, flow dynamics, and flow homogeneity and constituents, ρ_{df} is the average density of the mixture and v is the velocity of the flow front. To determine an approximate value of k , Armanini and Scotton (1993) carried out flume experiments with solid-fluid mixtures of different densities. They observed that when light granular material is present (i.e. anionic resin, $\rho = 1080 \text{ kg m}^{-3}$) gravity forces prevail, the flow still accelerates at the impact, a vertical jet forms and $k \sim 0.45$. If the material is denser (i.e. PVC mixture, $\rho = 1300 \text{ kg m}^{-3}$) then there is more internal friction, the flow decelerates at the front, a wave propagates upstream and $k \sim 2.2$. In the absence of direct observations on the impact of the flows at Sarno we adopted for k a value of 0.5 being mindful of the uncertainty in the value of this coefficient

(Keaton, 1990; Armanini and Scotton, 1993; Zhang, 1993; Coussot, 1997; Zanchetta et al., 2004). Thus, the computer application, which is described in the next section, requires from the user an average density of the mixture in kg m^{-3} and uses the velocity obtained from the equations in Table 3 to estimate dynamic pressure (kPa) according to Equation 10 with $k = 0.5$.

AUTOMATIC MAPPING OF DEBRIS FLOW VELOCITY AND DYNAMIC PRESSURE

This section describes a procedure that facilitates the production of velocity and/or dynamic pressure maps by using the equations presented earlier in this paper (Table 3; Equation 10). It constitutes a piece of software written in VBA that runs within ArcGIS® and is deployed as a template from which any ArcGIS® project can be derived.

The inputs required by the graphic-user interface (GUI) (Figure 7) are: (i) the height above the surface at the initiation point, (ii) the debris flow volume (m^3) or the depression angle ($^\circ$), (iii) a vector layer with the location of the starting point for inundation (i.e. apex of the alluvial fan or top of the scarp) and (iv) a digital elevation model (DEM). This application allows the user to model the velocity on the basis of any of the two equations based on energy lines starting at the apex of the alluvial fan (i.e. ApexG1 or ApexG2) (Table 3) or by user-defined coefficients (e.g. ScarpG1, ScarpG2, etc.) following the advanced option on the GUI (Figure 7). Output maps may be of velocity (m s^{-1}), dynamic pressure (kPa) or both. For the dynamic pressure the interface requires a density in kg m^{-3} and the code uses equation 10.

If the debris flow volume (V) is selected, then the code uses the equation $\Delta H/L = 3.29 V^{-0.28}$ (Toyos *et al.*, 2007b) to estimate the value of the Heim coefficient ($\Delta H/L$) and the equations based on the fan apex (Table 3) to predict velocity. Therefore, the starting point must be located at the lowermost part of the source area. The user decides whether the code uses ApexG1 or ApexG2 (Table 3) by checking or leaving unchecked the checkbox in the GUI (Figure 7). Otherwise, if the input is a depression angle, then the Heim coefficient results from the tangent of the angle. Runs of this application with the equa-

1
2 tions based on energy lines starting at the top of the scarp (i.e. ScarpG1 or ScarpG2) shall use as input
3
4 a depression angle until the volume-mobility ratio relationship can be improved (Toyos et al., 2007b).
5
6

7
8
9 The code uses the Heim coefficient to constrain both the distal limits of the flow and the Δh along the
10 path (Figure 5). It first finds the intersection of the energy line with the ground surface by assigning a
11 value of 1 to the cells for which $\Delta h > 0$ and a value of zero to those where Δh is negative. Then the
12 product between this grid and the raster that contains the values of Δh is calculated, resulting in a grid,
13
14 whose cells have either the value of Δh , if located within the distal limits of the flow or zero, other-
15 wise. The code uses this final grid as input for the calculation of debris flow velocity and this velocity
16 grid may be then used as input for the generation of a dynamic pressure layer. The output velocity
17 and/or dynamic pressure rasters are added to the ArcGIS ® table of contents (TOC) as layers rendered
18 with five classes. Overlaid onto this grid a vector layer is generated, which defines the maximum po-
19 tential extent of the flow (Figure 8).
20
21
22
23
24
25
26
27
28
29
30
31
32

33 DISCUSSION

34
35
36 The nature of the approach presented is essentially empirical-statistical (Rickenmann, 2005) and there-
37 fore, the whole modelling process, i.e. data collection and analysis, model formulation, statistical cali-
38 bration and GIS-implementation, involved important assumptions, simplifications and uncertainties,
39 which we intended to consider strictly. The advantages of the method proposed are typical of simple
40 approaches to complex natural phenomena: (i) trial-and-error calibration of rheological parameters by
41 doing back analysis is not necessary; (ii) its application is straightforward, and (iii) it requires a limited
42 number of parameters and modest computer resources. We did not implement other type of ap-
43 proaches such as a Voelmy type model (Ayotte and Hungr, 2000; Hungr et al., 2005; Rickenmann,
44 2005) because our key objective was to introduce a simple practical solution for rapid hazard mapping
45 of debris flows. With the model proposed users shall attempt to obtain first order approximations of
46 debris flow velocities and dynamic pressures and therefore, it shall complement rather than compete
47 with more rigorous physically based approaches.
48
49
50
51
52
53
54
55
56
57
58
59
60

1
2 We presented an approach that enables the prediction of the velocity of debris flows within reasonable
3 levels of uncertainty ($< 30\%$). However, its empirical-statistical nature (Rickenmann, 2005) con-
4 straints its application to similar geologic and geomorphic settings and moreover, the equations it uses
5 hold for small volume debris flows of low mobility (Iverson, 1997; Zanchetta *et al.*, 2004; Oramas
6 Dorta *et al.*, 2007; Toyos *et al.*, 2007b)
7
8
9
10
11
12

13
14
15 With regards to the two types of mobility considered, the statistical fits were better with the datasets
16 based on energy lines starting at the top of the scarps. This contrasts to the companion paper (Toyos *et*
17 *al.*, 2007b), which shows a better correlation between the flow volume and the mobility ratio, when
18 the ratios are based on energy lines starting at the apex of the alluvial fan (Toyos *et al.*, 2007b). Thus,
19 the calibrations based on the top of the scarps appear to account better for the exponential type decel-
20 eration of the velocity from the apex of the alluvial fan (Figure 2). It must be borne in mind that the
21 maximum Δh for energy lines starting at the top of the scarp coincides roughly in location with the fan
22 apex, where the peak discharge and the mean velocity at peak discharge were measured and used to
23 parameterise the velocity profiles.
24
25
26
27
28
29
30
31
32
33
34
35
36

37 Despite the limitations above mentioned, the statistical fits obtained for ApexG1 and ApexG2 were
38 acceptable and for modelling future debris flow events, the identification of the apex of the alluvial fan
39 is more straightforward than the top of the scarp of potential source areas. For these reasons, the com-
40 puter application presented uses by default the equations based on the fan apex. In this way, the user is
41 also able to model the velocity/dynamic pressure and maximum run-out of the same event, given also
42 the relationship between the flow volume and the mobility ratio (Toyos *et al.*, 2007b) that has been
43 also implemented (see previous section on the GIS implementation and Figure 7).
44
45
46
47
48
49
50
51
52
53

54 Another characteristic of the regression models based on energy lines starting at the apex of the allu-
55 vial fan is that the flow velocity is considerably underestimated at and near the apex. However, from a
56 hazard assessment perspective, this underestimation does not constitute a serious limitation, since
57 within the distal limits of the flow output maps based on these models are similar to those obtained
58
59
60

1
2 from the calibrations based on energy lines starting at the top of the scarps and the main interest is on
3
4 the built-up areas near the distal limits of the flow and not near the apex.
5
6

7
8
9 Finally, it is important to point out that output velocities/dynamic pressures correspond to the centre of
10 the flow path. In other words, velocities/pressures are predicted at each cell as if the centreline of the
11 flow path passed through that cell. At higher slopes near the apex of the alluvial fan the effect of to-
12 pography becomes stronger and therefore, the fan lines in between velocity categories are no perpen-
13 dicular to the centre line of the inundated area (Figures 8.a-d)
14
15
16
17
18

21 22 CONCLUSIONS

23
24
25
26 The analysis of velocity profiles revealed two main types of flow behaviour partly explained by the
27 variability in the density of infrastructure. Despite the heterogeneity in flow morphology and behav-
28 iour and the indirect nature of the velocity measurements, it was possible to calibrate a set of regres-
29 sion models that enable the prediction of debris flow velocity with an associated uncertainty of < 30%.
30
31 It was interesting to find that a simple approach such as the energy line concept could serve as a
32 framework for the calibration of velocities. The results justify the assumption that all the factors that
33 induce resistance to motion and force the flow to stop can be accounted for by the two coefficients of
34 the regression line (Equation 6). Although it could be argued that the models are under specified, the
35 resulting equations enable the objective prediction of debris flow velocities within reasonable levels of
36 uncertainty. However, it is still necessary to improve the characterisation and classification of flow
37 behaviours, the statistical fits and the precision of the model predictions with more data on past events.
38
39 This work should be replicated in other settings and with data on debris flows of larger magnitudes
40 and mobilities than the events that occurred in Southern Campania. Cross-validation experiments with
41 numerical models would also extend the scope of hazard assessment investigations.
42
43
44
45
46
47
48
49
50
51
52
53
54
55
56
57

58
59 Finally, the GIS-implementation, using commercially available software and user-friendly GUIs, en-
60 ables the rapid production of maps of debris flow velocity and dynamic pressure. Despite the subjec-
tivity in the parameterisation of the inputs for the models (i.e. volumes or depression angles, location

1
2 of the apex of the alluvial fan, digital topography), the approach presented here constitutes an impor-
3 tant step forward towards real-time hazard mitigation in regions mantled by volcanic deposits, where
4 mass-wasting phenomena such as debris flows represent a major hazard. The software is available
5 upon request and we expect to make it public in ESRI's website in the near future.
6
7
8
9

10 11 12 13 14 15 16 17 18 19 20 21 22 23 24 25 26 27 28 29 30 31 32 33 34 35 36 37 38 39 40 41 42 43 44 45 46 47 48 49 50 51 52 53 54 55 56 57 58 59 60

ACKNOWLEDGEMENTS

This research constitutes a portion of the work carried out by the first author towards the PhD degree at the University of Cambridge, England, which was funded and supported by Fundación YPF – Argentina, the Department of Geography of Cambridge University, King's College Cambridge and the Cambridge Overseas Trust. We also thank the Italian National Research Council (CNR), the Italian Institute of Geophysics and Volcanology (INGV), the University of Pisa (Italy) and the Vesuvian Observatory for providing funding, data and support in the field. Thanks very much to the two anonymous reviewers, who provided invaluable comments, suggestions and criticism that contributed towards a substantial improvement of the manuscript.

REFERENCES

- Armanini A, Scotton P. 1993. On the dynamic impact of a debris flow on structures. *Proceed. of XXV Congress of IAHR, Technical session B, Debris flows and Landslides 3*: 203 – 210.
- Ayotte D., Hungr O. 2000. Calibration of a run-out prediction model for debris flows and avalanches. In: *Proceed. 2nd International Conference on Debris-Flow Hazards Mitigation: Mechanics, Prediction and Assessment*, Wieckzorek GF, Naeser ND (eds), Taipei, Taiwan: 505 – 514.
- Baxter P. 2000. Human and structural vulnerability assessment for emergency planning in a future eruption of Vesuvius using volcanic simulation and casualty modelling. *Final Report Synthesis. Environmental and Climate Programme 1994-1998. EC-Project ENV4-CT98-069*.
- Bulmer MH, Barnouin-Jha OS, Peitersen MN, Bourke M. 2002. An empirical approach to studying debris flows: Implications for planetary modeling studies. *Journal of Geophysical Research* 107 (E5): 10.1029/2001JE001531.

- 1
2
3
4
5
6
7
8
9
10
11
12
13
14
15
16
17
18
19
20
21
22
23
24
25
26
27
28
29
30
31
32
33
34
35
36
37
38
39
40
41
42
43
44
45
46
47
48
49
50
51
52
53
54
55
56
57
58
59
60
- Calcaterra D, Parise M, Palma B, Pelella L. 2000. Multiple debris-flows in volcanoclastic materials mantling carbonate slopes. *Proceed. Second International Conference on Debris-Flow Hazards Mitigation: Mechanics, Prediction and Assessment*: 99 – 107, Taipei, Taiwan.
- Chow VT. 1959. *Open – channel hydraulics*. Mc. Graw – Hill, New York.
- Coussot P. 1997. *Mudflow Rheology and Dynamics*. IAHR Monograph, Balkema, Rotterdam.
- Corominas J. 1996. The angle of reach as a mobility index for small and large landslides. *Can. Geotech. J.* 33: 260 – 271.
- Crosta GB, Dal Negro PD. 2003. Observations and modelling of soil slip-debris flow initiation processes in pyroclastic deposits: the Sarno 1998 event. *Natural Hazards and Earth System Sciences* 3: 53 – 69.
- de Riso R, Budetta P, Calcaterra D, Santo A. 1999. Le colate rapide in terreni piroclastici del territorio campano. *Atti. Conv. Previsione e Prevenzione di Movimenti Franosi Rapidi*: 133 – 150, Trento, Italy (in Italian).
- Denlinger RP, Iverson RM. 2001. Flow of variably fluidised granular masses across three-dimensional terrain 2. Numerical predictions and experimental tests. *Journal of Geophysical Research* 106 (B1): 553 – 566.
- Di Vito MA, Sulpizio R, Zanchetta, G. 1998. I depositi ghiaiosi della valle dei Torrenti Clanio e Acqualonga (Campania Centro – Orientale): Significato stratigrafico e ricostruzione paleoambientale. *Quaternario* 11: 273 – 286 (in Italian).
- García R, López JL, Noya M, Bello ME, Bello, MT, González N, Paredes G, Vivas, MI. 2003. Hazard mapping for debris-flow events in the alluvial fans of northern Venezuela. In: *Proceed. Third International Conference on Debris-Flow Hazards Mitigation: Mechanics, Prediction and Assessment* 1, Rickenmann D, Cheng-lung C (eds), Davos, Switzerland: 589 – 599.
- Guadagno FM, Celico PB, Esposito L, Perriello Zampelli S, Piscopo V, Scarascia-Mugnozza G. 1999. The Debris Flows of 5-6 May 1998 in Campania, Southern Italy. *Landslide News* 12: 5 – 7.
- Hayashi JN, Self S. 1992. A comparison of Pyroclastic Flow and Debris Avalanche Mobility. *Journal of Geophysical Research* 97(B6): 9063 – 9071.
- Heim A. 1882. *Z. Dtsch. Geol. Ges.* 34, 74; *Bergsturz und Menschenleben* (Zürich, 1932) (in German).

- 1
2 Hsü J. 1975. Catastrophic debris streams (sturzsstroms) generated by rockfalls. *Geological Society of*
3
4 *America Bulletin* 86: 129 – 140.
5
6
7 Hungr O, Corominas J, Eberhardt E. 2005. Estimating landslide motion mechanism, travel distance
8 and velocity. In *Proceed. International Conference on Landslide Risk Management, Vancouver*. Hungr
9 O, Fell R, Couture R, Eberhardt E. (eds), Leiden: A.A. Balkema: 99 – 128
10
11
12 Hungr O, Morgan GC, Kellerhals R. 1984. Quantitative analysis of debris torrent hazards for design of
13 remedial measures, *Canadian Geotechnical Journal* 21: 663 – 677
14
15
16
17 Iverson RM. 1997. The physics of debris flows. *Reviews of Geophysics* 35: 245 – 296.
18
19
20 Iverson RM. 2003. The debris flow rheology myth. In: *Proceed. Third International Conference on*
21 *Debris-Flow Hazards Mitigation: Mechanics, Prediction and Assessment 1*, Rickenmann D, Cheng-
22 lung C (eds), Davos, Switzerland: 303 – 314.
23
24
25
26 Iverson RM, Denlinger RP. 2001. Flow of variably fluidised granular masses across three-dimensional
27 terrain: 1. Coulomb mixture theory. *Journal of Geophysical Research* 106 (B1): 537 – 552.
28
29
30 Iverson, RM, LaHusen, RG, Major, JJ, Zimmerman, CL. 1994. Debris flows against obstacles and
31 bends: Dynamic and deposits. *EOS Trans. AGU*: 75, 274.
32
33
34
35 Johnson AM, Rodine JR. 1984. Debris Flow. In: *Slope Instability*, Brundsen D, Prior DB (eds): 257 –
36 361.
37
38
39 Keaton JR. 1990. Predicting alluvial-fan sediment-water slurry characteristics and behaviour from
40 sedimentology and stratigraphy of past deposits. In: *Hydraulics/Hydrology of Arid Lands*, French RH
41 (ed), ASCE, New York: 608 – 613.
42
43
44
45 Körner HJ. 1976. Reichweite und Geschwindigkeit von Bergstürzen und fleischneelawinen. *Rock me-*
46 *chanics* 8: 225 – 256.
47
48
49
50 Kover TP. 1995. *Application of a digital terrain model for the modelling of volcanic flows: A tool for*
51 *volcanic hazard determination*. Unpublished MSc. Thesis, University of New York at Buffalo, USA.
52
53
54
55 Macedonio G, Pareschi MT. 1992. Numerical simulation of some lahars from Mount St. Helens.
56 *Journal of Volcanology and Geothermal Research* 54: 65 – 80.
57
58
59 Malin MC, Sheridan MF. 1982. Computer-Assisted Mapping of Pyroclastic Surges. *Science* 217: 637
60 – 640.

- 1
2
3
4
5
6
7
8
9
10
11
12
13
14
15
16
17
18
19
20
21
22
23
24
25
26
27
28
29
30
31
32
33
34
35
36
37
38
39
40
41
42
43
44
45
46
47
48
49
50
51
52
53
54
55
56
57
58
59
60
- McEwen M, Malin MC. 1989. Dynamics of Mt. St. Helens' 1980 pyroclastic flows, rockslide-avalanche, lahars and blast. *Journal of Volcanology and Geothermal Research* 37: 205 – 231.
- Mizuyama T, Ishikawa Y. 1990. Prediction of debris flow prone areas and damage. In: *Hydraulics/Hydrology of Arid Lands. Proceedings International Symposium*, French RH (ed), ASCE (New York): 712 – 717.
- O'Brien JS, Julien PY, Fullerton WT. 1993. Two-dimensional water flood and mudflow simulation. *Journal of Hydraulic Engineering* 119: 244 – 261.
- Onorati G, Braca G, Iritano, G. 1999. Evento idrogeologico del 4, 5 e 6 maggio 1998 in Campania. Monitoraggio e analisi idrologica. *Atti.Acc. Naz. Lincei* 154: 103-108 (in Italian).
- Oramas Dorta D, Toyos G, Oppenheimer C, Pareschi MT, Sulpizio R, Zanchetta G. 2007. Empirical modelling of the May 1998 small debris flows in Sarno (Italy) using LAHARZ. *Natural Hazards* 40: 381 – 396.
- Pareschi MT, Favalli M, Giannini F, Sulpizio R, Zanchetta G, Santacroce R. 2000. May 5, 1998, debris flows in circumvesuvian areas (Southern Italy): Insights for hazard assessment. *Geology* 7 : 629 – 642.
- Pareschi MT, Santacroce R, Sulpizio R, Zanchetta G. 2002. Volcaniclastic debris flows in the Clanio Valley (Campania, Italy): insights for the assessment of the hazard potential. *Geomorphology*: 43: 219 – 231.
- Pescatore T, Ortolani F. 1973. Schema tettonico dell'Appennino campano-lucano. *Boll. Soc. Geol. Ital.* 92: 453 – 473 (in Italian).
- Pierson TC. 1995. Flow characteristics of large eruption-triggered debris flows at snow-clad volcanoes: Constraints for debris-flow models. *Journal of Volcanology and Geothermal Research* 66: 283 – 294
- Pierson TC, Janda RJ, Thouret JC, Borrero, CA. 1990. Perturbation and melting of snow and ice by the 13 November 1985 eruption of Nevado del Ruiz, Colombia, and consequent mobilisation, flow and deposition of lahars. *Journal of Volcanology and Geothermal Research* 41: 17 – 66.
- Porfido S, Esposito E, Alaia F, Esposito G, Laccarino G. 2002. Ill dissesto idrogeologico: inventario e prospettive. *Atti. Accademia Nazionale dei Lincei* 181: 457 – 466.
- Rickenmann D. 1999. Empirical relationships for debris flows. *Natural Hazards* 19: 47 – 77.

1
2 Rickenmann D. 2005. Run-out prediction methods. In: Jakob M, Hungr O (eds), *Debris-Flow Hazards*
3 *and Related Phenomena* Praxis-Springer, Heidelberg: 263-282

4
5
6 Rickenmann D, Koch T. 1997. Comparison of debris flow modelling approaches. In: *Proceed. First*
7 *International Conference on Debris-Flow Hazards Mitigation: Mechanics, Prediction and Assess-*
8 *ment*: Cheng-lung C (ed), San Francisco (California), USA: 576 – 585.

9
10 Sheridan M, Malin M. 1983. Application of computer-assisted mapping to volcanic hazard evaluation
11 of surge eruptions: Vulcano, Lipari. *Journal of Volcanology and Geothermal Research* 17: 187 – 202.

12
13 Sheridan M., Macías JL. 1992. PC Software for 2-Dimensional gravity-driven flows: Applications to
14 the Colima and El Chichón volcanoes, Mexico. *Proceed. 2nd Reunion Int. Volcanol*, Colima, Mexico:
15 5.

16
17 Sheridan MF, Hubbard B, Carrasco-Nuñez G, Siebe C. 2000. GIS model for volcanic hazard assess-
18 ment: pyroclastic flows at Volcán Citlaltépetl, México. In: *Proceed. 4th international conference on in-*
19 *tegrating geographic information systems and environmental modeling: problems, prospects, and*
20 *needs for research*, Parks BO, Clarke KM, Crane MP (eds), Boulder, University of Colorado, USA.

21
22 Siebert L. 1984. Large volcanic debris avalanches: Characteristics of source areas, deposits and asso-
23 ciated eruptions. *Journal of Volcanology and Geothermal Research* 22: 163 – 197.

24
25 Spence RJS, Baxter PJ, Zuccaro G. 2004. Building vulnerability and human casualty estimation for a
26 pyroclastic flow: a model and its application to Vesuvius. *Journal of Volcanology and Geothermal Re-*
27 *search* 133: 321 – 343.

28
29 Toyos G, Cole P, Felpeto A, Martí J. 2007_a. A GIS-based methodology for hazard mapping of small
30 volume pyroclastic flows. *Natural Hazards* 41: 99 – 112

31
32 Toyos G, Oppenheimer C, Pareschi MT, Sulpizio R, Zanchetta G, Zuccaro G. 2003. Building damage
33 by debris flows in the Sarno area, Southern Italy. In: *Proceed. Third International Conference on De-*
34 *bris-Flow Hazards Mitigation: Mechanics, Prediction and Assessment 2*, Rickenmann D, Cheng-lung
35 C. (eds), Davos, Switzerland: 1209 – 1220.

36
37 Toyos G, Oramas Dorta D, Oppenheimer C, Pareschi MT, Sulpizio R, Zanchetta G. 2007_b. GIS-
38 assisted modelling for debris flow hazard assessment based on the events of May 1998 in the area of
39 Sarno, Southern Italy. Part I: Maximum run-out. *Earth Surface Processes and Landforms* (in press).

1
2 Valentine GA. 1998. Damage to structures by pyroclastic flows and surges, inferred from nuclear
3 weapons effects. *Journal of Volcanology and Geothermal Research* 87: 117-140.

4
5
6 Zanchetta G, Sulpizio R, Pareschi MT, Leoni FM, Santacroce R. 2004. Characteristics of May 5 – 6,
7 1998 volcanoclastic debris-flows in the Sarno area of Campania, Southern Italy: relationships to struc-
8 tural damage and hazard zonation. *Journal of Volcanology and Geothermal Research* 133: 377 – 393.

9
10
11 Zhang S. 1993. A comprehensive approach to the observation and prevention of debris flows in China.
12
13 *Natural Hazards* 7: 1 – 23.

14
15
16
17 Zuccaro G, Baratta A, Petrazzuoli S, Ianniello D, Baxter P.J, Spence, RJS. 2000. Structural vulnerabil-
18 ity to possible pyroclastic flows consequent to the Eruption of the Volcano Vesuvius. *Final Report EC*
19
20 *Project ENV4 – CT98 – 0699. Human and Structural Vulnerability Assessment for Emergency Plan-*
21
22 *ning in a Future Eruption of Vesuvius using Volcanic Simulation and Casualty Modelling.*
23
24
25
26
27
28
29
30
31
32
33
34
35
36
37
38
39
40
41
42
43
44
45
46
47
48
49
50
51
52
53
54
55
56
57
58
59
60

1
2
3
4
5
6
7
8
9
10
11
12
13
14
15
16
17
18
19
20
21
22
23
24
25
26
27
28
29
30
31
32
33
34
35
36
37
38
39
40
41
42
43
44
45
46
47
48
49
50
51
52
53
54
55
56
57
58
59
60

FIGURE CAPTIONS

Figure 1. Shaded relief of the Sarno area within the regional context. Grey indicates the source areas, white, the transport zones and black, the deposition areas. Two or more source areas (e.g. Lav-2) or two inundation areas that merged (e.g. Ep-6) were combined in this analysis. Velocity data were collected at channel bends and within the deposition areas of Ep-2, Ep-3, Ep-4, Ep-5, Ep-6, Ep-7, Lav-1, Lav-2, Quin-6 and Sia-2.

Figure 2. Normalised velocity (v/v_{\max}) ($\text{m s}^{-1}/\text{m s}^{-1}$) (above) and velocity (m s^{-1}) (below) against the fraction of total flow run-out distance (D/R) (m/m) for each basin. Groups I, II and III refers to the three sets of velocity profiles (see section *Longitudinal velocity profiles*)

Figure 3. Velocity measurements (m s^{-1}) in (a) Ep-2, Ep-3, Ep-4 and Ep-5, (b) Ep-6 and Ep-7 and (c) Lav-1 and Lav-2. White represents the transport zones, light grey the source areas and dark grey the deposition areas. The buildings are also in white and the black line in Ep-7 represents an artificial channel. Measurements in Ep-2 and Ep-4 have almost no buildings upstream. Despite the few buildings in Ep-5, a wall at the end of the main square (Piazza Duomo) and the streets decelerated the flow to velocities $< 5 \text{ m s}^{-1}$. Notice the proximity of the measurements in Ep-7 to the artificial channel. This may explain the high velocities reported.

Figure 4. Velocity measurements (m s^{-1}) in (a) Quin-6 and (b) Sia-2. Light grey represents the source areas, white the transport zones and dark grey the deposition areas. Note the low density of buildings (white polygons) surrounding the velocity of 10.5 m s^{-1} at Sia-2.

Figure 5. Diagram illustrating the estimation of debris flow velocity on the basis of the energy line concept (Hsü, 1975) and the parameters used to model the velocity, i.e. E_D = Euclidean distance from the starting point, $H_E = E_D \times \Delta H/L$, $H_{ALT} (\Delta H)$ = DEM-elevation + user-defined altitude above the source centre (a value slightly larger 0 might be required to avoid spurious results, when digital or natural topography surrounding the starting point blocks the energy line), H_T (energy line elevation) = $H_{ALT} - H_E$, $\Delta h = H_T - \text{DEM-elevation}$. All distances and elevations are in metres.

Figure 6. Velocity (v) (m s^{-1}) vs. distance between the energy line and the ground surface (Δh) (m) and the calibrations for both groups of datasets constrained: (a) with mobility ratios based on energy

1
2 lines starting at the apex of the alluvial fan and (b) with Heim coefficients based on energy lines start-
3
4 ing at the highest landslide scar. For the equations and regression results see Table 3.
5

6
7 **Figure 7.** Graphic-user interface (GUI) for the inputs to simulate debris flow velocity and/or dynamic
8
9 pressure.
10

11 **Figure 8.** Velocity for Ep-6: (a) with the calibration based on energy lines starting at the apex of the
12 alluvial fan, (ApexG1) ($\theta = 7.2^\circ$) and (b) with the equation based on energy lines starting at the highest
13 landslide scar, (ScarpG1) ($\theta = 15.9^\circ$); (c) Dynamic pressure based on the velocity shown by *a* and a
14 flow density of 1830 kg m^{-3} (Zanchetta *et al.*, 2004). The grids are shown within the perimeter of the
15 flow's inundation area, i.e. the output grids were cut using a polygon shapefile that defines the flow
16 inundation area. The black and white crosses in (a, c) and (b), respectively, represent the location of
17 the apex of the alluvial fan. In (a) and (c) this cross also indicates both the location of the apex of the
18 alluvial fan and the starting point for the simulation. In (b) the starting point was located further up-
19 stream from the apex at the highest landslide scar and therefore, the cross indicates only the apex of
20 the alluvial fan.
21
22
23
24
25
26
27
28
29
30
31
32
33
34
35
36
37
38
39
40
41
42
43
44
45
46
47
48
49
50
51
52
53
54
55
56
57
58
59
60

TABLES

Table 1. Volume, peak discharge, mean velocity at peak discharge (v_{\max}) at the apex of the alluvial fan, and morphology class (Figure 1; see also Table 1 in Toyos *et al.*, 2007b).

Basin	Volume (m^3)	Morphology	Q_p (m^3s^{-1})	v_{\max} (m s^{-1})
Ep_2	1.1×10^5	Simple	1.6×10^3	16
Ep_3	1.7×10^5	Complex	2.2×10^3	18
Ep_4	4.5×10^4	Simple	0.8×10^3	14
Ep_5	1.2×10^5	Simple	1.7×10^3	13
Ep_6	1.7×10^5	Complex	2.3×10^3	18
Ep_7	1.3×10^5	Complex	1.9×10^3	17
Lav_1	1.3×10^5	Simple	1.8×10^3	15
Lav_2	2.5×10^5	Complex	3.1×10^3	17
Quin_6	3.2×10^4	Simple	0.6×10^3	14
Sia_2	6.4×10^4	Complex	1.0×10^3	16

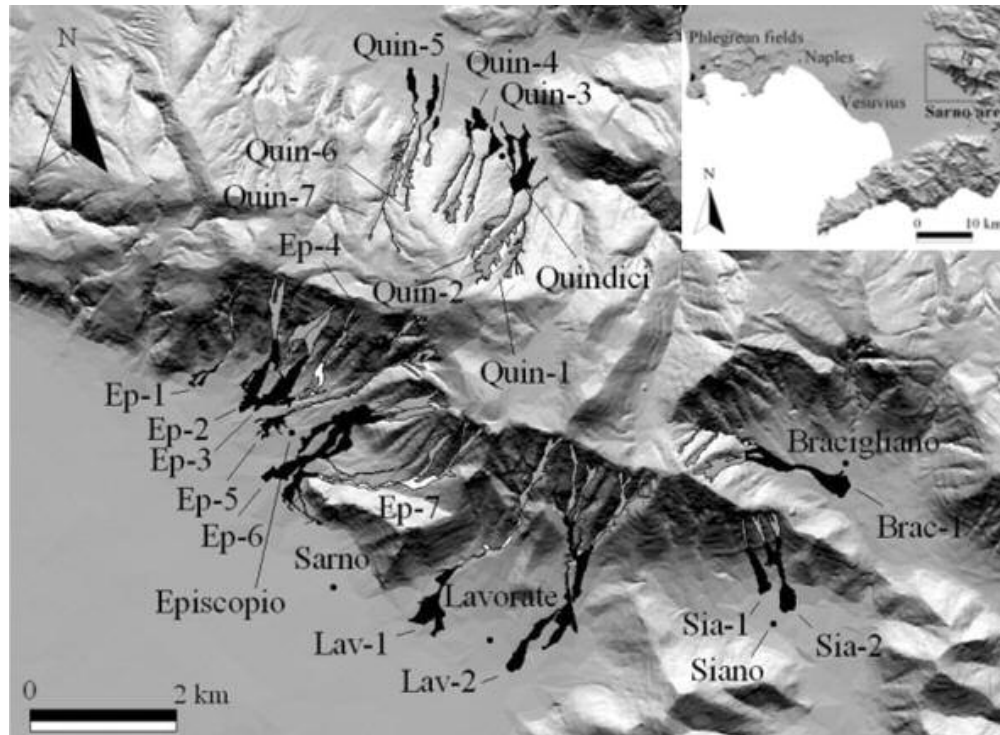
Table 2. Mobility ratios based on energy lines starting at the apex of the alluvial fan (θ_1) and on the top of the scarp (θ_2) and empirical data used in the statistical calibration: distance between the energy line and the surface (Δh) and velocity (v_{obs}). Mean velocities at peak discharge obtained from Equation 2 are in the 4th column. Velocities in the other columns were obtained from Equation 4, except for the ones in the 5th column of Ep-5 and Lav-1, which were obtained from Equation 3. For energy lines starting at the apex of the alluvial fan mean velocities at peak discharge were calculated a few hundred metres downstream the apex, while for energy lines starting at the top of the scarp these measurements were at the apex of the alluvial fan (for more details see text).

Basin	$\theta_1(^{\circ})$	Energy line starting at the apex of alluvial fan ($\Delta H/L_1$)									
		Δh									
Ep-2	7.3	Δh	27	16	12						
		v_{obs}	11.5	7.9	7.8						
Ep-3	7.0	Δh	33	20							
		v_{obs}	10.1	5							
Ep-4	10.2	Δh	34	11	11						
		v_{obs}	10.1	7.9	6.2						
Ep-5	8.4	Δh	49	29	25	21	14				
		v_{obs}	12.5	11.1	5	4.9	3.5				
Ep-6	7.2	Δh	59	39	44	43	39	31	25	25	20
		v_{obs}	14.6	9	7	5.5	5.9	5.8	5.4	5.4	3
Ep-7	8.6	Δh	47	20	19	16	15				
		v_{obs}	12.4	7.9	6.1	7.9	9.5				
Lav-1	6.7	Δh	52	44	29						
		v_{obs}	12.4	15	4.4						
Quin-6	9.2	Δh	65	55							
		v_{obs}	10.1	6.4							
Sia-2	7.0	Δh	65	32	27	25	28				
		v_{obs}	12.1	10.5	4	5.4	2.1				
Basin	$\theta_2(^{\circ})$	Energy line starting at the highest landslide scar ($\Delta H/L_2$)									
Ep-2	18.9	Δh	224	56	41						
		v_{obs}	15.9	7.9	7.8						
Ep-3	19.6	Δh	223	64							
		v_{obs}	17.9	5							
Ep-4	21.9	Δh	185	44	39						
		v_{obs}	14.4	7.9	6.2						
Ep-5	16.4	Δh	277	99	75	51					
		v_{obs}	12.6	5	4.9	3.5					
Ep-6	16.1	Δh	279	144	114	82	117	58	63	33	
		v_{obs}	18.2	7	5.9	5.8	5.5	5.4	5.4	3	
Ep-7	16.9	Δh	234	42	61	52	40				
		v_{obs}	16.8	9.5	7.9	7.9	6.1				
Lav-1	15.4	Δh	325	82							
		v_{obs}	15.1	4.4							
Quin-6	16.1	Δh	167	130							
		v_{obs}	14.5	6.4							
Sia-2	25.1	Δh	161	49	36	45					
		v_{obs}	16.5	10.5	5.4	4					

Table 3. Regression results for both sets of mobility ratios and the two groups of flow events, one with low (Group I) and the other with high velocities (Group I) at the lower values of Δh (see Figure 6).

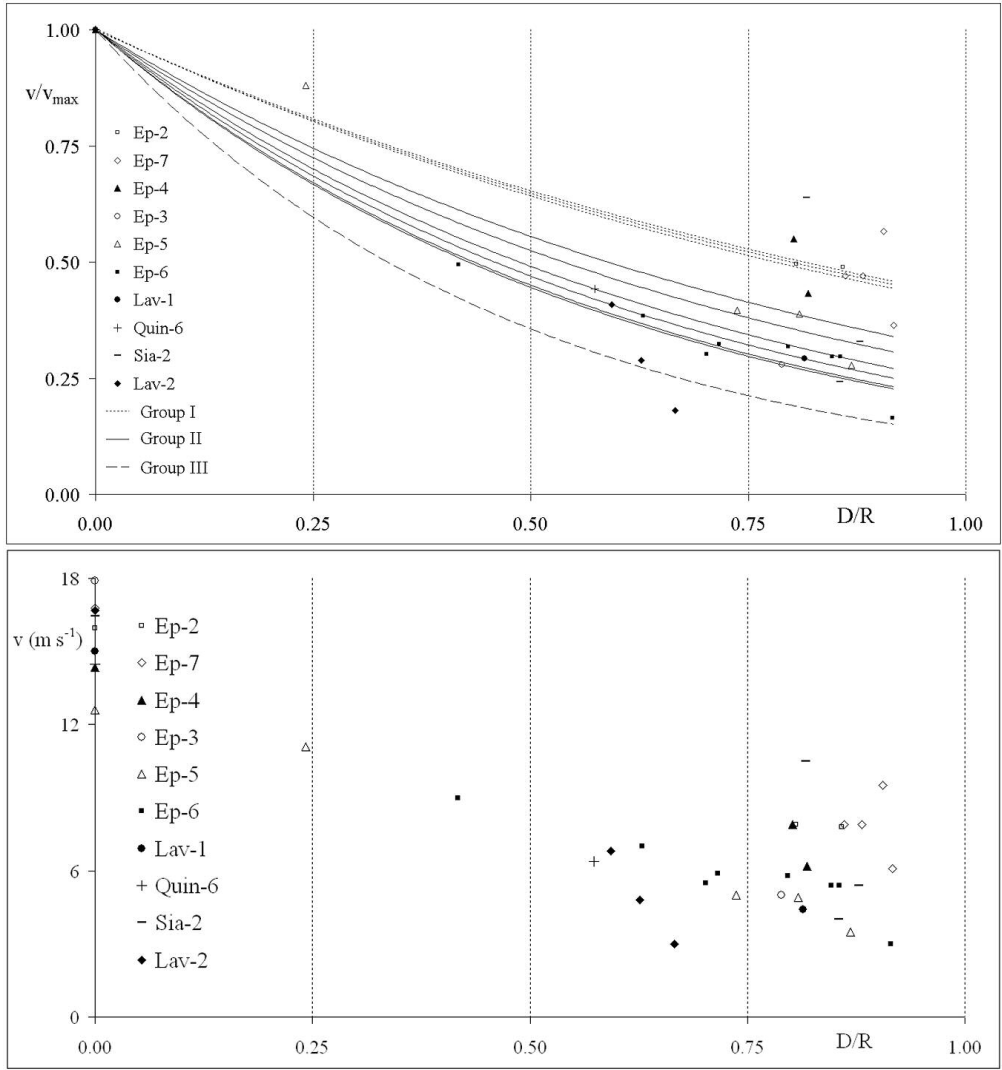
Mobility based on...	...apex of alluvial fan		... highest landslide scar	
	ApexG1 *	ApexG2 *	ScarpG1	ScarpG2
Equation	$v = 0.28 \Delta h^{0.91}$	$v = 2.9 \Delta h^{0.37}$	$v = 0.27 \Delta h^{0.71}$	$v = 1.25 \Delta h^{0.47}$
nr. observations	26	11	26	11
r^2	0.49	0.59	0.68	0.90
Standard error (SE)	0.16	0.07	0.15	0.05
p	< 0.01	< 0.01	< 0.01	< 0.01
slope (a)	0.91	0.37	0.71	0.47
slope - 95%	0.54	0.14	0.51	0.35
slope + 95%	1.28	0.60	0.90	0.59
slope - 90%	0.60	0.18	0.54	0.37
slope + 90%	1.22	0.56	0.87	0.57
intercept (log(a))	-0.56	0.46	-0.57	0.10
intercept - 95%	-1.13	0.16	-0.97	-0.13
intercept + 95%	0.01	0.76	-0.17	0.32
intercept - 90%	-	-	-0.90	-0.08
intercept + 90%	-	-	-0.24	0.28

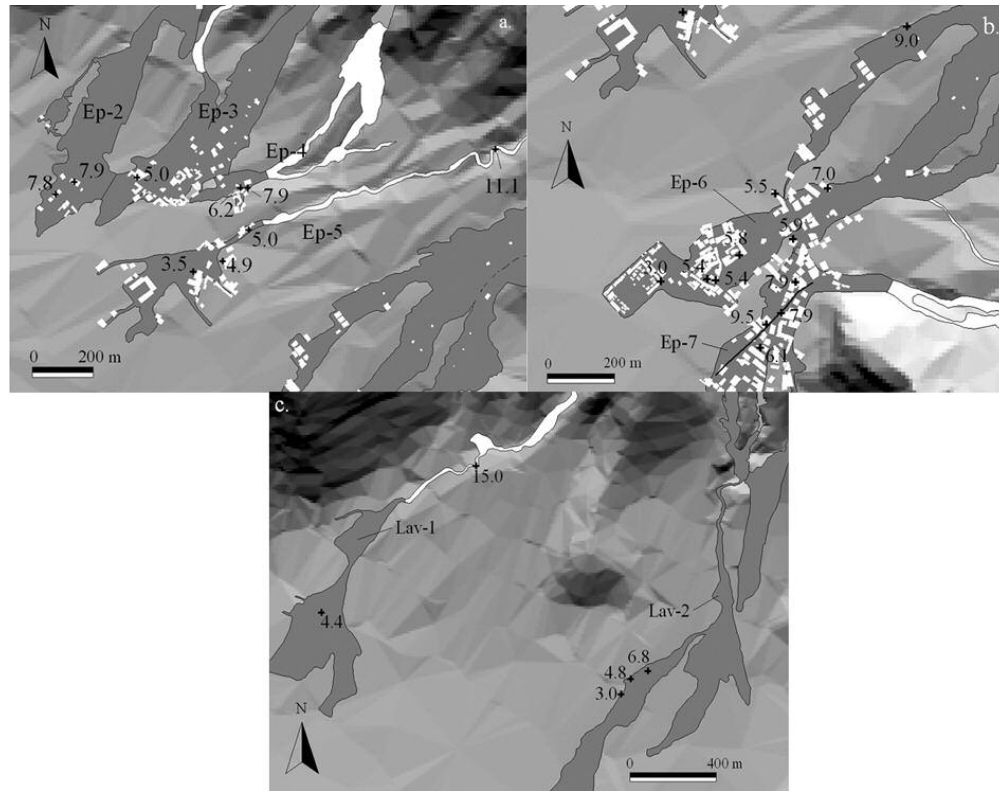
* 90% and 95% indicate the level of confidence



Shaded relief of the Sarno area within the regional context. Grey indicates the source areas, white, the transport zones and black, the deposition areas. Two or more source areas (e.g. Lav-2) or two inundation areas that merged (e.g. Ep-6) were combined in this analysis. Velocity data were collected at channel bends and within the deposition areas of Ep-2, Ep-3, Ep-4, Ep-5, Ep-6, Ep-7, Lav-1, Lav-2, Quin-6 and Sia-2.

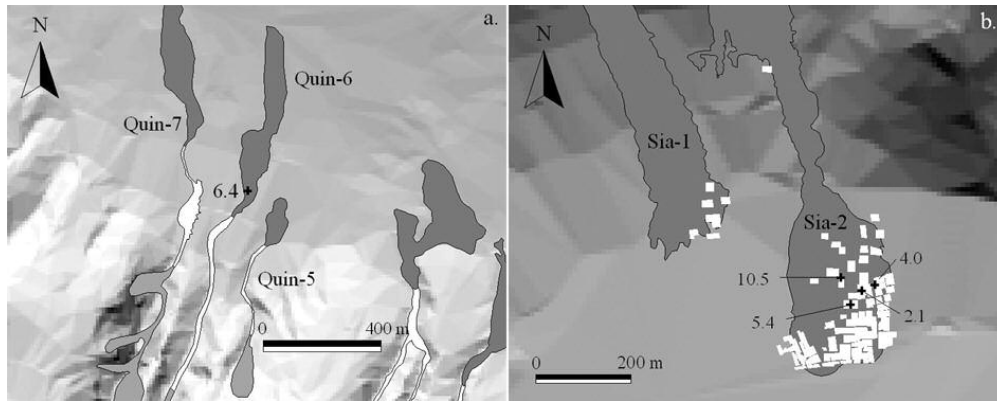
1
2
3
4
5
6
7
8
9
10
11
12
13
14
15
16
17
18
19
20
21
22
23
24
25
26
27
28
29
30
31
32
33
34
35
36
37
38
39
40
41
42
43
44
45
46
47
48
49
50
51
52
53
54
55
56
57
58
59
60





Velocity measurements (m s^{-1}) in (a) Ep-2, Ep-3, Ep-4 and Ep-5, (b) Ep-6 and Ep-7 and (c) Lav-1 and Lav-2. White represents the transport zones, light grey the source areas and dark grey the deposition areas. The buildings are also in white and the black line in Ep-7 represents an artificial channel. Measurements in Ep-2 and Ep-4 have almost no buildings upstream. Despite the few buildings in Ep-5, a wall at the end of the main square (Piazza Duomo) and the streets decelerated the flow to velocities $< 5 \text{ m s}^{-1}$. Notice the proximity of the measurements in Ep-7 to the artificial channel. This may explain the high velocities reported.

1
2
3
4
5
6
7
8
9
10
11
12
13
14
15
16
17
18
19
20
21
22
23
24
25
26
27
28
29
30
31
32
33
34
35
36
37
38
39
40
41
42
43
44
45
46
47
48
49
50
51
52
53
54
55
56
57
58
59
60



Velocity measurements (m s⁻¹) in (a) Quin-6 and (b) Sia-2. Light grey represents the source areas, white the transport zones and dark grey the deposition areas. Note the low density of buildings (white polygons) surrounding the velocity of 10.5 m s⁻¹ at Sia-2.

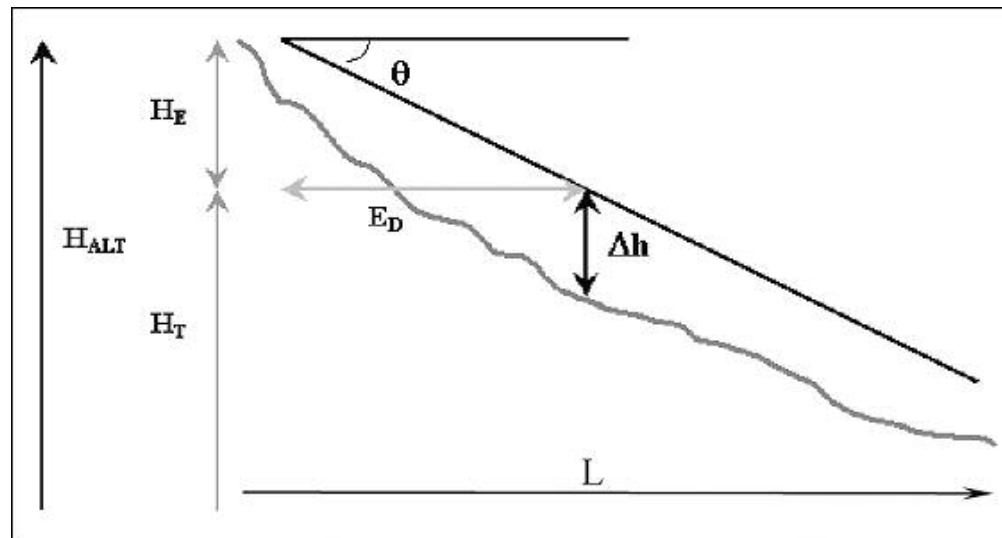
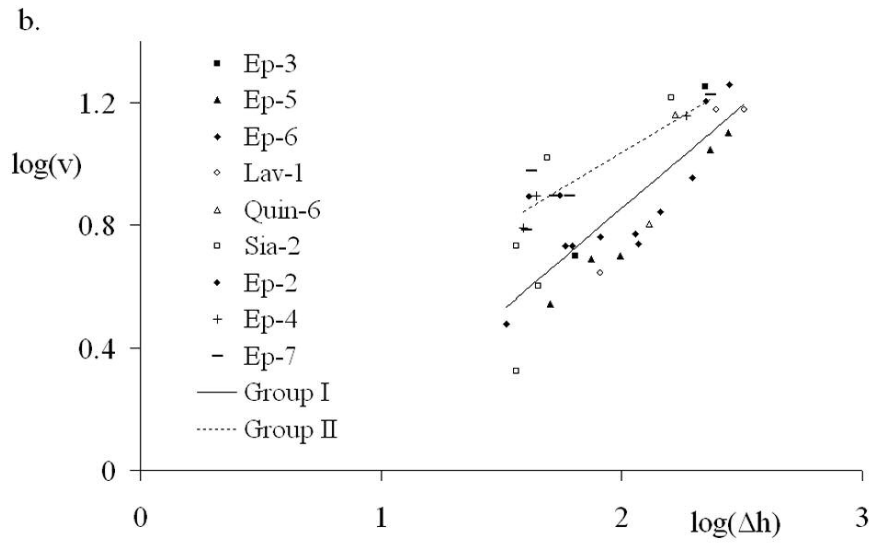
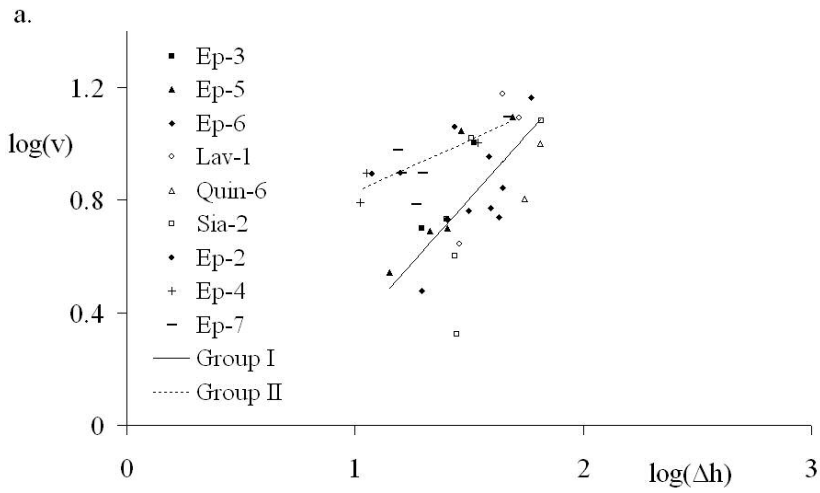


Diagram illustrating the estimation of debris flow velocity on the basis of the energy line concept (Hsü, 1975) and the parameters used to model the velocity, i.e. E_D = Euclidean distance from the starting point, $H_E = E_D \times \Delta H/L$, H_{ALT} (ΔH) = DEM-elevation + user-defined altitude above the source centre, H_T (energy line elevation) = $H_{ALT} \square H_E$, $\Delta h = H_T \square$ DEM-elevation. All distances and elevations are in metres.



90x110mm (300 x 300 DPI)

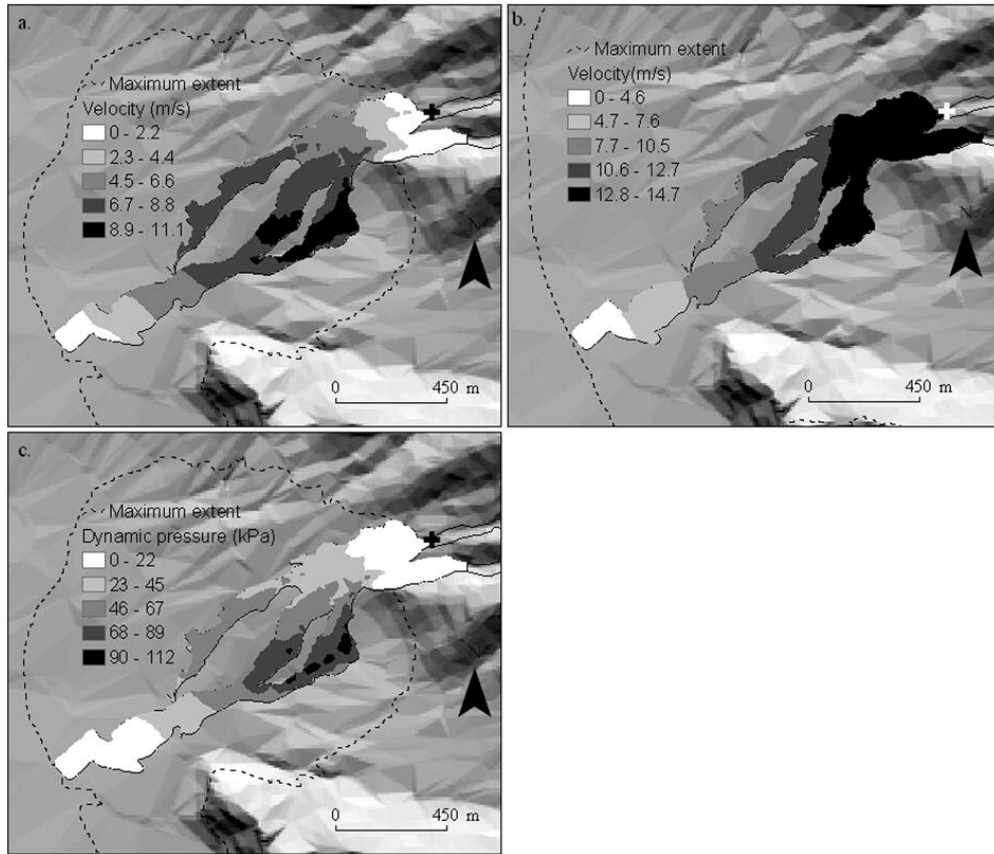
1
2
3
4
5
6
7
8
9
10
11
12
13
14
15
16
17
18
19
20
21
22
23
24
25
26
27
28
29
30
31
32
33
34
35
36
37
38
39
40
41
42
43
44
45
46
47
48
49
50
51
52
53
54
55
56
57
58
59
60

The image shows two overlapping windows from a software application. The top window, titled 'Debris flow hazard assessment', contains two buttons: 'Maximum extent' and 'Velocity & Dynamic pressure'. The bottom window, titled 'Debris flow velocity and dynamic pressure', is the active window and contains the following controls:

- Main parameters:**
 - 'Height of source above surface (m):' with a text box containing '0'.
 - 'Debris flow volume (c.m.):' with a radio button and a text box containing 'N/A'.
 - 'Depression angle (degrees):' with a radio button (selected) and a text box containing '7.2'.
- Output Type:**
 - 'Velocity (m/s) (Flow Group II)' with a radio button and a button labeled 'Advanced'.
 - 'Dynamic pressure (kPa) - Density (kg/c.m.):' with a radio button (selected) and a text box containing '1830'.
- Name of the source and elevation layers:**
 - 'Source layer:' with a text box containing 'START'.
 - 'Elevation layer:' with a text box containing 'DEM'.
 - A button labeled 'RUN'.

Graphic-user interface (GUI) for the inputs to simulate debris flow velocity and/or dynamic pressure.

1
2
3
4
5
6
7
8
9
10
11
12
13
14
15
16
17
18
19
20
21
22
23
24
25
26
27
28
29
30
31
32
33
34
35
36
37
38
39
40
41
42
43
44
45
46
47
48
49
50
51
52
53
54
55
56
57
58
59
60



80x68mm (300 x 300 DPI)

view